JOURNAL OF Materials CHEMISTRY

Nanocrystalline iron-doped mesoporous titania and its phase transition

Yu-Hong Zhang[a,b] **and Armin Reller***[a]

[a]*Solid State Chemistry, Institute of Physics, University of Augsburg, 86135 Augsburg, Germany. E-mail: armin.reller@physik.uni-augsburg.de; Tel: 0049-821-5983000*
[b]*Department of Chemistry, Zhejiang University, Hanzhou 310027, China*

Received 26th April 2001, Accepted 17th July 2001
First published as an Advance Article on the web 7th September 2001

Nanocrystalline mesoporous iron-doped TiO_2 was prepared as a single-phase product by a novel sol–gel technique. By transmission, scanning and analytical electron microscopy as well as by complementary techniques it has been found that the as-prepared solids exhibit a narrow size distribution and that the iron is homogeneously distributed in the TiO_2 matrix. The influence of the iron concentration on the phase transformations of the doped TiO_2 was investigated by X-ray diffractometry. The formation of the iron titanium oxide pseudobrookite, $Fe_2Ti_2O_5$, was observed above 670 °C, but only for an iron content of more than 3 atom%. UV-spectroscopic measurements reveal that the absorption spectrum of the iron doped titania is sensitively related to both the iron concentration and the calcination temperature. Whereas pure nanocrystalline TiO_2 undergoes grain growth (sintering) when the calcination temperature is increased, iron doped TiO_2 proves to be inert to grain growth. N_2 adsorption–desorption analysis indicated that the products calcined between 390 and 600 °C for 1 h in air have mesoporous structure and the distribution of mesopores is very narrow, centered at 3.7 nm.

1. Introduction

Nanocrystalline titanium dioxide finds a broad spectrum of realized and potential applications in the areas of photocatalysis, photovoltaics and photochromics.[1–3] However, titanium dioxide only absorbs 5% of the spectrum of the incoming sunlight in the near ultraviolet region which clearly limits its efficient application. Numerous studies have been performed to extend the photoresponse of TiO_2 and to improve its photoactivity by modifying its surface properties, composition, *etc.*[4–7] Selective doping of the crystalline matrix has been proven to be an efficient route to improve the photoactivity of semiconducting oxides, and for titania the effect is dramatic when it is doped with various transition metal cations.[8–11] Fe(III) in a metal oxide matrix is sensitive to visible light and iron-doped TiO_2 has been found to exhibit an increased quantum efficiency for the photoreduction of nitrogen.[10] In addition, the lifetime of the hole–electron pairs for other photocatalytic reactions is augmented.[9,12] On the other hand, it has been widely demonstrated that some properties of pure and doped TiO_2, especially its photocatalytic properties, are very sensitive to changes of the crystal structure, *i.e.* the electronic structure.[13–15] Together with the crystal structure, the size of crystalline domains and the morphology of the individual particles, the homogeneous distribution and integration of dopants in the structural framework play the key role for the optimization of specific photoelectrochemical and catalytic properties. However, to our knowledge, a systematic detailed description of structural phase transformations and temperature dependent changes of the particle sizes of iron-doped TiO_2 has not yet been reported. A possible reason may be that synthesis methods such as co-precipitation, ion exchange or wet impregnation are conventionally used for preparing doped titania. Applying these methods, however, not only is tedious but it is also difficult to prepare homogeneously doped TiO_2 or to control grain growth. The high-temperature diffusion technique used to form homogeneously doped TiO_2 readily causes complete structural transformation from the anatase to the rutile modification.

In this paper, we report a novel route for preparing nanocrystalline iron doped TiO_2. This synthesis allows the tailoring of the crystal structure modification and the particle size of iron doped titania by controlling the calcination temperature. Particle growth induced by high temperature calcination can be significantly restrained by iron doping.

2. Experimental

Butane-1,4-diol (>98%, Merck) was added to a beaker containing $Fe(NO_3)_3{\cdot}9H_2O$ (>98%, Merck) according to the required iron dopant amounts: 0, 1, 2, 3, 4, 5 and 6 atom% (leading to samples denoted TF0, TF1, TF2, TF3, TF4, TF5 and TF6, respectively). Subsequently titanium isopropoxide (98%, Aldrich) was added at room temperature with constant stirring. The mixture was aged at ambient temperature for a few days. During this time the liquid became progressively more viscous and eventually a dry gel formed. Crystallization was achieved by subsequent calcination of the dry gel in air at different temperatures using the same heat treatment program for all samples. The crystallinity and the structure/modification of the products were studied on a Phillips Xpert X-ray diffractometer using Cu-Kα radiation. Investigations of particle morphology and nanostructure were performed on a CM-30 transmission electron microscope (TEM) and the micrographs were recorded at 300 kV. The samples were prepared by dispersing the powder products as a slurry in heptane, which was then deposited and dried on a holey carbon film mounted on a Cu grid. The iron distribution was determined by an energy dispersive X-ray detector (EDX) which was mounted in a LEO-982 scanning electron microscope (SEM). UV-absorption measurements were performed using a Shimadzu UV-2401 PC spectrophotometer. Nitrogen sorption data were collected on a Micromeritics ASAP2000

Sorption Analyzer. Pore size distributions were modeled using the BJH method from the desorption data.

3. Results and discussion

The activity of iron-containing TiO_2 is strongly influenced by the iron content, and many experiments have demonstrated that titania with low iron content shows enhanced reactivity.[5] We prepared a series iron-doped titania with iron content ranging from 1 to 6 atom%. In the initial stage of the preparation, the iron and titanium precursor compounds were homogeneously dispersed in butane-1,4-diol and a transparent liquid formed. The subsequent sol–gel process took place over a few days and led to a homogeneous dispersion. Either pure or homogeneously doped nanocrystalline titania was finally obtained by appropriate heat treatments. EDX investigations (*via* SEM or TEM mode) gave evidence that the iron dopant is homogeneously distributed in the TiO_2 matrix, either in the anatase or rutile modification (Fig. 1). Typical electron micrographs for sample TF6 calcined at 600 °C for 1 h in air are presented in Fig. 2(a) and (b). Comparison with pure titania subjected to the same calcination procedure (Fig. 2(c)) shows that the particle size of the iron doped titania is much more uniform and much smaller, with an average diameter of 14 nm. It is evident that the particle growth becomes restrained upon iron doping, which is of significant importance not only for the design of surface properties and surface area, but also in tuning the electronic structure.[16]

The absorption spectrum, *i.e.* the color of the iron-doped TiO_2 can be tuned as a function of the iron content and/or the final calcination temperature from yellow to bright brown through to dark brown. Fig. 3 shows UV absorption spectra of selected samples with various iron contents exposed to different calcination temperatures. It can be seen that the absorption range is progressively broadened when the iron content increases. On the other hand, high calcination temperatures cause an increased spectral absorption.

Three well defined crystallographic modifications of titania are known to occur naturally: brookite, anatase and rutile. X-Ray diffraction (XRD) is an efficient method to identify the exact crystal structures and modifications of pure and iron-doped TiO_2. Fig. 4 shows the dependence of the phase transformation temperatures of pure and iron-doped nanocrystalline TiO_2. The transition of pure TiO_2 from the amorphous state to anatase is observed at a lower temperature than for iron doped titania. It is also important to note that for pure TiO_2 the transformation from anatase to rutile takes place at 500 °C, *i.e.* at much lower temperatures than that of iron-doped

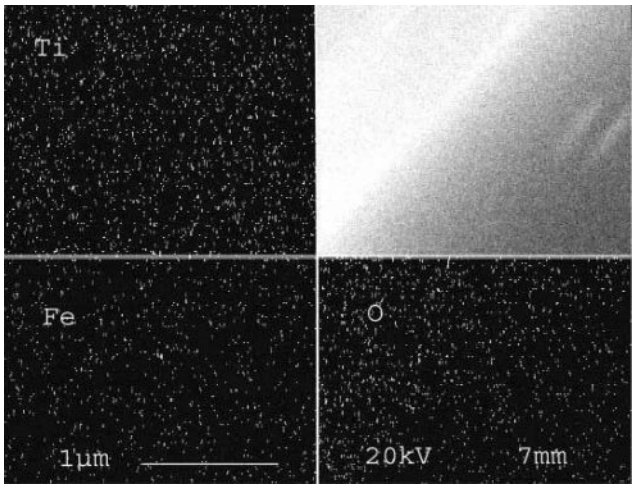

Fig. 1 Energy-dispersive X-ray mapping image scan of TF6 heated at 600 °C for 1 h which reveals a homogeneous iron distribution in the titania matrix.

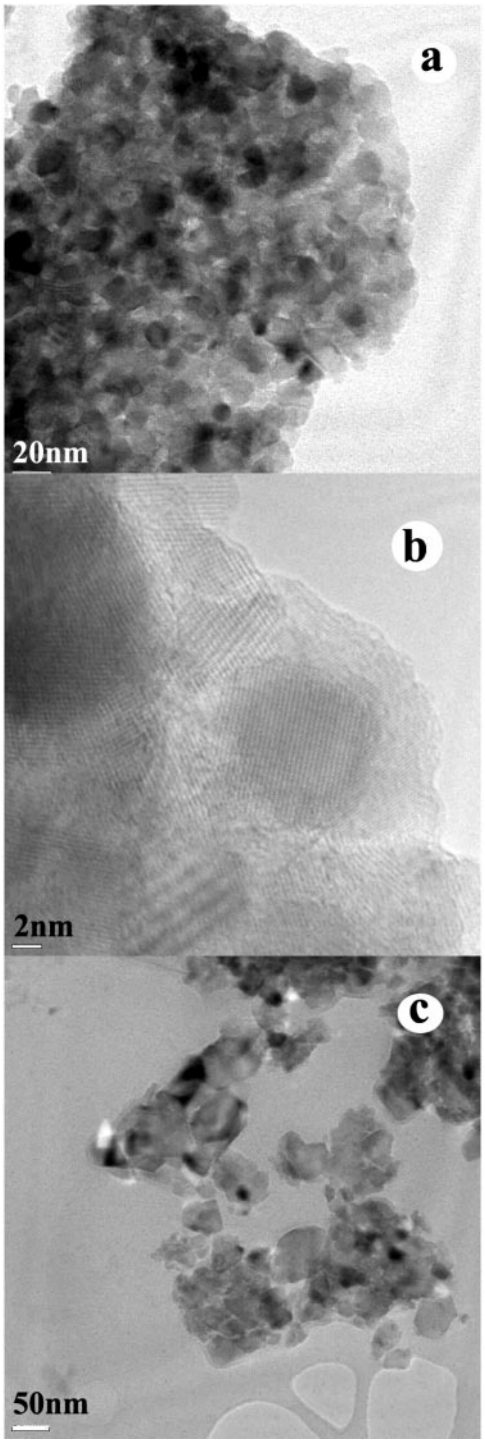

Fig. 2 HRTEM micrographs of pure and iron-doped titania products calcined in air at 600 °C for 1 h. (a), (b) HRTEM micrographs of TF6. (c) HRTEM micrograph of TF0.

TiO_2 (transition temperature: 600 °C). It is evident that the remarkable shift of crystallization and of the phase transition from anatase to rutile to higher temperatures is caused by structural iron doping, *i.e.* the substitution of titanium ions by iron ions within the structural framework. It is noteworthy that at the end of the anatase to rutile transformation of iron-doped nanocrystalline TiO_2 with an iron doping of more than 3 atom%, the iron titanium oxide pseudobrookite, $Fe_2Ti_2O_5$, is formed. Upon exploring the X-ray diffraction patterns no indication could be found for the formation of binary iron oxide(s). These findings are consistent with the results obtained by EDX: in all doped iron is homogeneously distributed in the titania matrix.

The XRD pattern of TF6 annealed at 830 °C for 1 h is

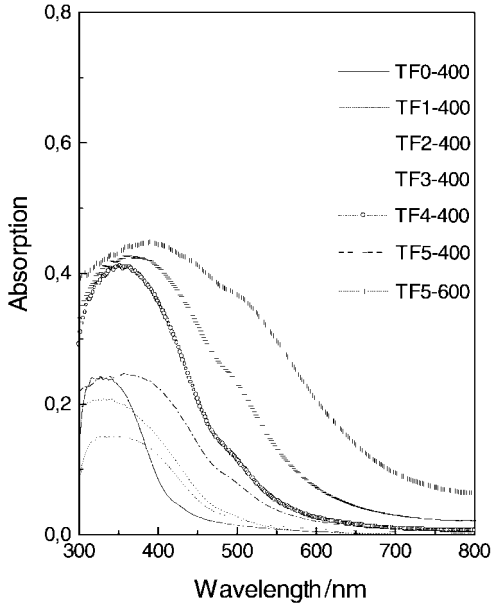

Fig. 3 UV-absorption spectra of TF0–5 calcined at 400 °C for 1 h and of TF5 calcined at 600 °C for 1 h.

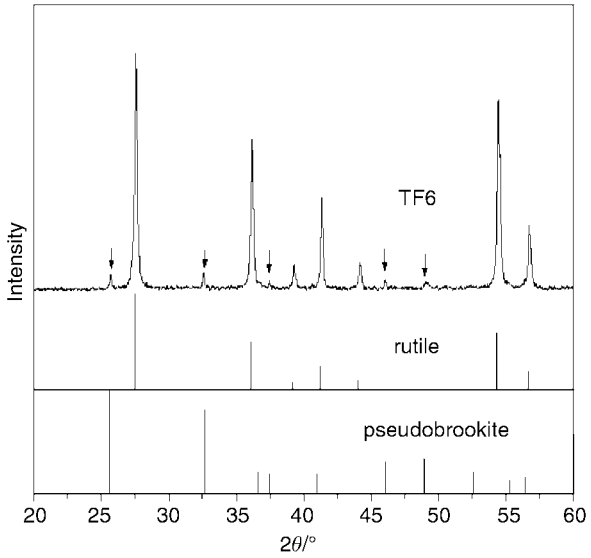

Fig. 5 X-Ray diffraction pattern of TF6 calcined at 830 °C for 1 h. The reflections for rutile and iron titanium oxide (pseudobrookite) are also shown for comparison.

shown in Fig. 5. Four new, well-resolved peaks with 2θ values of 25.62, 32.50, 37.39 and 45.97°, and one new, broad peak with a 2θ value of 48.99° are observed. Using the PCPDF database, we found that these new peaks can be attributed to iron titanium oxide (pseudobrookite). The relative intensity of these peaks did not change when TF6 was calcined at 1000 °C for 1 h. Therefore, it is evident that all the doped iron is transformed into iron titanium oxide at 830 °C. When the calcination temperature was less than 650 °C, no iron oxide nor iron titanium oxide peaks were detected, indicating that the iron was completely integrated in the titania structure.

Fig. 6 shows the changes of the relative peak intensities of TF6 in the range $20° < 2\theta < 30°$. The (101) reflection of anatase is observed at $2\theta = 25.27°$, the (110) reflection of rutile at $2\theta = 27.75°$ and an iron titanium oxide (pseudobrookite) peak at $2\theta = 25.62°$. The intensity of the rutile (110) reflection increases slightly when the calcination temperature is changed from 600 to 630 °C, indicating a slow rate for the phase transformation. However, this signal intensifies rapidly above 630 °C. When the calcination temperature reaches 650 °C, rutile becomes the dominant phase. In addition a small shoulder neighboring the (101) reflection of anatase around $2\theta = 25.62°$ emerges. This reflection demonstrates the evolution of the iron titanium oxide phase in the TF6. After calcination at 670 °C, the weak diffraction peak of the iron titanium oxide phase is intensified relative to the anatase (101) reflection. Upon further increasing the calcination temperature to 700 °C, the anatase (101) reflection disappears, indicating the completion of the anatase to rutile transition. In samples treated by this procedure the pseudobrookite reflection also becomes more distinct.

The content of iron doped in the titania matrix apparently influences the evolution of the pseudobrookite phase. Fig. 7 shows the XRD patterns of iron doped TiO_2 (TF1–TF6) calcined at 670 °C for 1 h. A weak shoulder attributed to iron

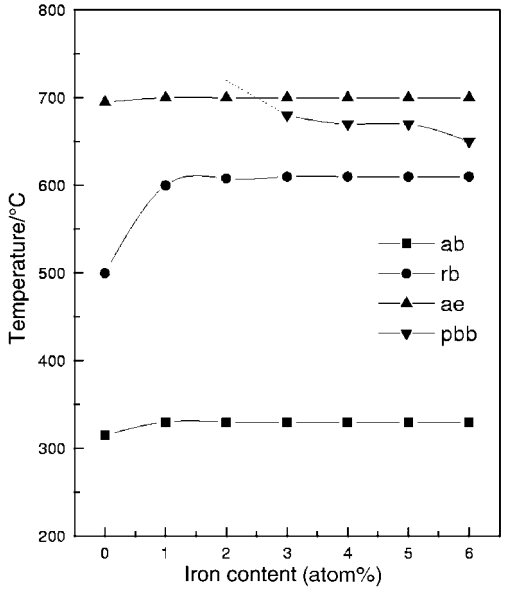

Fig. 4 Phase transformation temperatures of iron-doped titania. ab—the emergence of anatase; rb—the emergence of rutile; ae—the end of transformation of anatase to rutile; pbb—emergence of pseudobrookite.

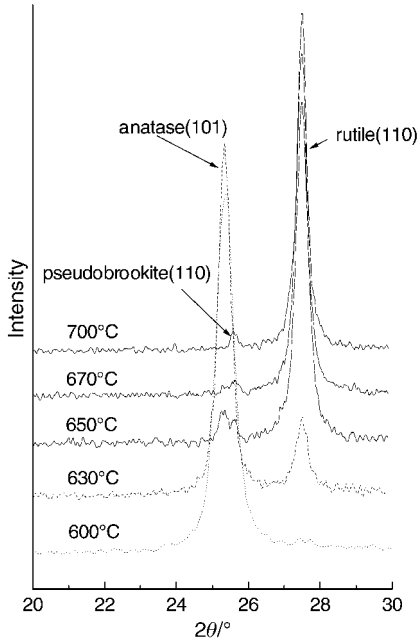

Fig. 6 X-Ray diffraction patterns of TF6 calcined at different temperatures for 1 h in air.

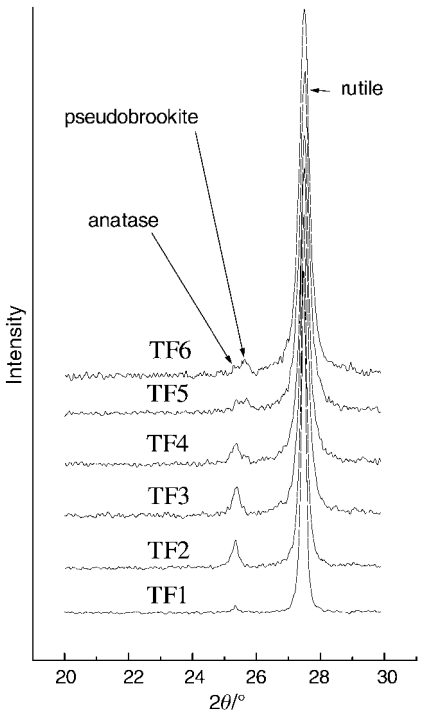

Fig. 7 X-Ray diffraction patterns of iron-doped nanoscopic TiO_2 samples (TF1–6) heated at 670 °C for 1 h in air.

titanium oxide appears in the XRD pattern of TF4, and the intensity of this peak increases with increasing iron content (TF5, TF6). No iron titanium oxide phase was observed in samples TF1, TF2 or TF3. When the calcination temperature of TF3 reached 690 °C, an iron titanium oxide peak at $2\theta = 25.62°$ emerges, indicating that the formation of the iron titanium oxide phase depends on both iron content and calcination temperature. However, only anatase and rutile peaks were observed for samples TF1 and TF2 calcined at all temperatures. It is clear that the evolution of the iron titanium oxide phase is sensitive to the quantity of doped iron. The higher the amount of iron, the earlier the evolution of pseudobrookite is observed. According to the current state on known properties (ref. 5 and references therein), the activity of the iron-doped titania is directly influenced by two important factors, *i.e.* the phase present and the iron distribution. Samples with optimal homogeneous distribution of iron in the titania matrix show a tendency to higher activity. However, the presence of hematite and pseudobrookite in the titania samples decreases the activity drastically.

Particle growth is observed at high calcination temperatures for the nanocrystalline particles due to their high surface energy. Compared with pure titania, iron-doped titania is more resistant to particle growth at increased temperatures. Using Scherrer's equation average particle sizes of the different samples calcined at 600 °C for 1 h have been determined (as shown in Table 1). Pure titania samples calcined at 600 °C for 1 h exhibit a particle size around 30 nm, while for 6 atom% iron doped titania samples calcined at the same temperature the corresponding value is around 14 nm. On increasing the iron content, the tendency to arrest grain growth is more evident. The average particle sizes calculated from XRD peak broadening are consistent with those determined by TEM. The

Table 1 Average grain sizes of the products TF0–TF6 calcined at 600 °C for 1 h determined by XRD and TEM methods

Sample	TF0	TF1	TF2	TF3	TF4	TF5	TF6
Size/nm	29.8	20.6	16	16	15.7	14.9	14.4

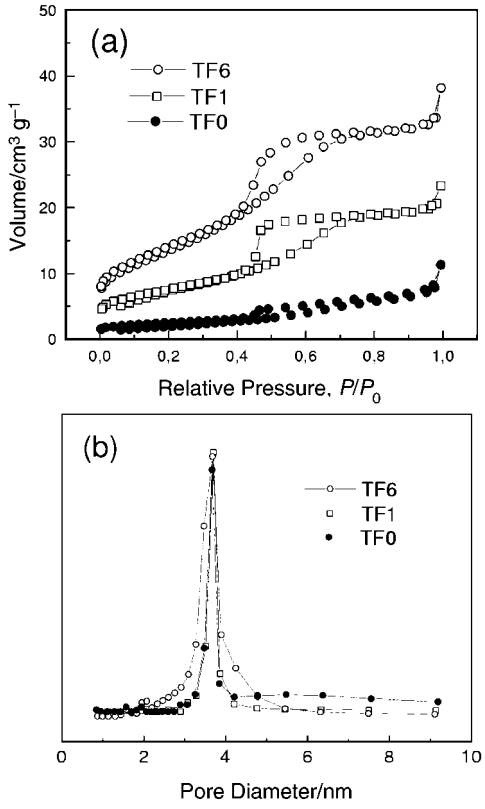

Fig. 8 (a) N_2 adsorption–desorption isotherms and (b) pore size distributions of TF0, TF1 and TF6 (from the desorption branch). The samples was calcined at 500 °C for 1.5 h.

results show that iron doping decreases grain growth rate, *i.e.* sintering. This trend is further confirmed by nitrogen adsorption–desorption analysis. Fig. 8 shows nitrogen sorption isotherms and pore size distribution curves of samples with various iron contents calcined at 500 °C. The isotherms as shown in Fig. 8(a) are of type IV (IUPAC, 1985) with an H2 hysteresis loop, which is a typical indication for a network of mesopores. The BJH analysis (Fig. 8(b)) yields a corresponding peak at a pore diameter of 3.71 nm, indicating a very narrow distribution of the mesopore dimensions. However, the surface areas clearly decrease with increased calcination temperature (Table 2). At calcination temperatures close to 600 °C, pure TiO_2 underwent drastic densification leading to a surface area reduction to 1.9 $m^2 g^{-1}$. A remarkable observation is that the surface area of iron doped samples is always higher than that of pure TiO_2 (for the same heating program). For example, the mesoporous structure and a large surface area (23.3 $m^2 g^{-1}$) is still maintained for TF6 upon calcination at 600 °C for 1 h. There is no doubt that the high surface area of iron doped samples is due to the decreased grain size, which is consistent with the results of XRD and TEM.

Table 2 Surface area, pore size and particle size from samples with different iron content at various calcination temperatures

Iron content (atom%)	Temperature/ °C	Time/ h	Surface area/ $m^2 g^{-1}$	Average pore radius/nm	Average particle diameter/nm
0	400	3	79	3.7	10.1
6	400	3	96	3.7	9.3
0	500	1.5	7.03	3.7	20.3
1	500	1.5	28.04	3.7	13.5
6	500	1.5	48.9	3.7	12.1
0	600	1	1.9	–	30
6	600	1	23.3	3.7	14.4

4. Conclusion

The synthesis of a series of homogeneous iron doped nanocrystalline TiO_2 samples by a novel sol–gel route provides a simple straightforward access to homogeneous iron-doped titania exhibiting promising properties for photocatalytic applications. The phase transition diagram presented here (Fig. 4) can be used as a basis for both controlled product formation and for optimization of structure–morphology–property relations as prerequisites for applications. It has also been found that the UV-absorption range of nanosized titania can be significantly broadened by iron doping. The grain size and the crystal structure or modification of the doped titania can be controlled by tailoring the calcination temperature. The crystal structure transformation of nanophase titania is influenced significantly by iron doping. The formation or segregation of the iron titanium oxide phase pseudobrookite depends on both the iron content and the calcination temperature. XRD and TEM results indicate that the iron doping decreases the grain growth rate, *i.e.* sintering processes, and therefore leads to higher surface areas.

Acknowledgements

We acknowledge Dr A. Weidenkaff for inspiring discussions and Dr O. Becker for recording HRTEM images.

References

1 P. V. Kamat, in *Nanoparticles and Nanostructured Films*, ed. J. H. Fendler, Wiley-VCH, New York, 1998.
2 B. O'Regan and M. Grätzel, *Nature*, 1991, **353**, 737.
3 M. Fröba, O. Muth and A. Reller, *Solid State Ionics*, 1997, **101–103**, 249.
4 M. R. Hoffmann, S. T. Martin, W. Choi and D. W. Bahnemann, *Chem. Rev.*, 1995, **95**, 56.
5 M. I. Litter and J. A. Navio, *J. Photochem. Photobiol. A*, 1996, **98**, 171.
6 G. H. Li, L. Yang, Y. X. Jin and L. D. Zhang, *Thin Solid Films*, 2000, **368**, 163.
7 C. C. Wang, Z. Zhang and J. Y. Ying, *Nanostruct. Mater.*, 1997, **9**, 583.
8 K. E. Karakitsou and X. E. Verykios, *J. Phys. Chem.*, 1993, **97**, 1184.
9 M. Graetzel and R. F. Howe, *J. Phys. Chem.*, 1990, **94**, 2566.
10 J. Soria, J. C. Conesa, V. Augugliaro, L. Palmisano, M. Schiavello and A. Sclafani, *J. Phys. Chem.*, 1991, **95**, 274.
11 J. Kiwi and C. Morrison, *J. Phys. Chem.*, 1984, **88**, 6146.
12 D. Bockelmann, R. Coslich and D. Bahnemann, in *Solar Thermal Energy Utilization*, ed. M. Becker, K. H. Funken and G. Schneider, Springer-Verlag Gmbh, Heidelberg, vol. 6, p. 397.
13 D. D. Beck and R. W. Spiegel, *J. Mater. Res.*, 1992, **7**, 2840.
14 G. Deo, A. M. Turek, I. E. Wachs, T. Machej, J. Haber, N. Das, H. Eckert and A. M. Hirt, *Appl. Catal., A*, 1992, **91**, 27.
15 R. J. Berry and M. R. Mueller, *Microchem. J.*, 1994, **50**, 28.
16 A. J. Nozik, in *Photocatalytic Purification and Treatment of Water and Air*, ed. D. F. Ollis and H. Al-Ekabi, Elsevier Science Publishers, New York, 1993, p. 39.